Environmental Science Processes & Impacts

ROYAL SOCIETY OF CHEMISTRY

PAPER

View Article Online
View Journal | View Issue

Cite this: *Environ. Sci.: Processes Impacts*, 2020, **22**, 1368

Photochemical fate of quaternary ammonium compounds in river water†

Priya I. Hora and William A. Arnold *

Received 20th February 2020
Accepted 16th April 2020

DOI: 10.1039/d0em00086h

rsc.li/espi

Quaternary ammonium compounds (QACs) are not completely removed during wastewater treatment and are frequently detected in surface waters and sediments. The photochemical transformation of QACs has not been thoroughly investigated as a potential degradation pathway affecting their fate in the environment. Kinetic studies of common QACs with and without aromatic groups under simulated and natural sunlight conditions were performed with model sensitizers and dissolved organic matter to estimate photochemical half-lives in the aquatic environment. All QACs investigated react with hydroxyl radicals at diffusion-controlled rates (~2.9×10^9 to 1.2×10^{10} M^{-1} s^{-1}). Benzethonium reacted *via* direct photolysis ($\Phi_{BZT,outdoor} = 1.7 \times 10^{-2}$ (mol Ei^{-1})). Benzethonium also reacted with the triplet excited state model sensitizer 2-acetylnaphthalene, but evidence suggests this reaction pathway is unimportant in natural waters due to faster quenching of the triplet 2-acetylnapthalene by oxygen. Reactivity with singlet oxygen for the QACs was minimal. Overall, reactions with hydroxyl radicals will dominate over direct photolysis due to limited spectral overlap of sunlight emission and QAC absorbance. Photolysis half-lives are predicted to be 12 to 94 days, indicating slow abiotic degradation in surface water.

Environmental significance

Quaternary ammonium compounds (QACs) are extensively used worldwide. The photochemical fate of QACs in aquatic environments is not fully understood. The present study comparatively evaluates the contributions of direct and indirect photolysis on the transformation of five QACs in the environment. Through a series of sensitizer experiments in buffer and river water experiments under simulated and natural sunlight, this work reveals that QACs are susceptible to indirect photolysis by hydroxyl radicals, but direct photolysis is only important for benzethonium. This study aids in assessing the role of photolysis in the overall fate of QACs in surface waters.

1. Introduction

Since the late 1930s, quaternary ammonium compounds (QACs) have been a widely used class of chemicals, chemical mixtures, and additives in a variety of industrial, agricultural, clinical, and consumer product applications.[1–3] Some QACs are designated by the U.S. Environmental Protection Agency and the Organization for Economic Cooperation and Development as high production volume chemicals (≥1 million pounds per year imported or manufactured). An extensive primary use of QACs is as cationic surfactants.[4,5] QACs are used in fabric softeners, antistatic agents, commercial disinfectants, sanitizers, antimicrobials, biocides, herbicides, pesticides, food preservatives, detergents, and phase transfer agents, and active ingredients in pharmaceuticals, cosmetics, and personal care products such as shampoos and antibacterial soaps.[1,2,6,7] QACs are also used as lytic biocides, corrosion inhibitors, and clay stabilizers in hydraulic fracturing.[6,8–10]

QACs contain at least one hydrophobic hydrocarbon chain bonded to a positively charged quaternary nitrogen atom and have other alkyl groups that tend to be mostly short-chain substituents such as methyl or benzyl functional groups.[1,11] The central nitrogen is covalently bonded to four carbon-containing "R"-substituents (R_4N^+).[6] There are three major classes of QACs: benzylalkyl dimethyl ammonium compounds (BACs), alkyltrimethyl ammonium compounds (ATMACs), and dialkyldimethyl ammonium compounds (DADMACs).

QACs are introduced into aquatic ecosystems through point source pollution and the discharge of effluents from wastewater treatment plants and are considered emerging pollutants.[1,2,7,12–16] QACs have been detected in environmental compartments ranging from surface water to sediments and may be found in septic and sewage impacted areas.[7,8,17–19] The worldwide average concentration of QACs in domestic wastewater, treated effluents, and surface water has been reported to be approximately 500 μg L^{-1}, 50 μg L^{-1}, and 40 μg L^{-1}, respectively.[3,13,20] The three QAC classes most frequently detected in the environment are: DADMACs with alkyl chain lengths

Department of Civil, Environmental, and Geo- Engineering, University of Minnesota – Twin Cities, 500 Pillsbury Drive SE, Minneapolis, Minnesota 55455, USA. E-mail: arnol032@umn.edu; Fax: +1-612-626-7750; Tel: +1-612-625-8582

† Electronic supplementary information (ESI) available. See DOI: 10.1039/d0em00086h

from C_8 to C_{18}, ATMACs with alkyl chain lengths from C_{12} to C_{18}, and BACs with alkyl chain lengths from C_{12} to C_{18}.[1] Approximately 75% of QACs used annually are released into wastewater treatment systems and BAC is the most frequently found QAC group worldwide in municipal wastewater effluents at concentrations ranging from 20 to 300 μg L^{-1}.[14,19,21–23] Although a large fraction of QACs are removed during the wastewater treatment process, QACs are still detected in aquatic environments, especially at higher concentrations in locations downstream of wastewater effluent discharge.[9,13,17,18,20,24–26]

Understanding the fate of QACs is important because an estimated 32.5% of QACs produced worldwide are released into the environment,[3] and they retain their biocidal properties after application.[3,27–29] QACs are known to be aerobically biodegradable, but the extent of biodegradation is variable.[4,8,30–32] Based on laboratory studies, rates can vary from hours to months and depend on factors such as QAC structure, concentration, and microbial acclimation.[33–36] Results from some of these studies suggest that biodegradation rates decrease with increasing hydrophobic alkyl chain length. Additionally, the data indicate that QACs with a benzyl group have decreased biodegradation.[8] Moreover, while water-soluble, QACs have a strong tendency to sorb to organic matter in water bodies due to favorable hydrophobic and electrostatic interactions,[7,17,18,37] which might reduce bioavailability and inhibit biodegradation. QACs have been detected in sediments at concentrations higher than in the aqueous phase,[18–20,24,38] suggesting that QACs are environmentally persistent[8] and their transport and fate are dependent upon association with organic matter in surface waters.[38]

Ecotoxicological effective concentrations (EC_{50}) of QACs reported for various fish, algae, crustaceans, daphnia, rotifers, and bacterial, and protozoan species range from tens of μg L^{-1} to mg L^{-1}.[1,2,32,39,40] While QACs generally have not been considered acutely toxic to aquatic organisms based on reported surface water concentrations below many EC_{50} values, more research is needed.[2,7,39] QACs might still pose cumulative chronic effects. Concerns about the detection of QACs in the environment stem from the possibility that prolonged exposure to sub-inhibitory QAC concentrations co-selects for antibiotic resistant bacteria.[3,28,41–45]

The photochemical behavior of QACs in natural environments is still not well understood. BACs are considered stable to direct photodegradation.[6,46] Direct photolysis occurs when a contaminant undergoes transformation, such as breaking of bonds, resulting from directly absorbing light energy.[47] Many QACs lack chromophoric functional groups or exhibit poor absorption of light in the visible spectrum; thus, direct photolysis processes may be limited in natural waters. Indirect photolysis, facilitated by QAC association with dissolved organic matter (DOM), could be an important and understudied attenuation mechanism. Indirect photolysis occurs when a photosensitizer such as organic matter in natural waters absorbs light energy, becomes electronically excited, and subsequently reacts with a contaminant or produces transient photochemically produced reactive intermediates (PPRIs) that are energetically capable of transforming target contaminants.[47] PPRIs, including reactive oxygen species (ROS), such as hydroxyl radicals ($^{\bullet}OH$) and singlet oxygen ($^1O_2$), and non-ROS excited triplet states of DOM ($^3DOM^*$), react with contaminants in natural systems thus enhancing degradation and increasing phototransformation rates.[47–50] QACs may sorb to DOM, which is ubiquitous in natural waters, and this interaction affects their distribution, transformation, and bioavailability. In aquatic systems, DOM may act as a sink for QACs and as a photosensitizer. For some hydrophobic compounds, attachment to DOM can expose the pollutant to heterogeneous microenvironments with high concentrations of PPRIs[51] that accelerate degradation, or alternatively, this association could shield compounds from light, inhibiting reactions.

This study examines the photochemical fate of 5 QACs in surface waters and addresses gaps in knowledge on biocide degradation.[6] By conducting experiments in buffered ultrapure water using sensitizers and radical quenchers and in Mississippi River water, the relative contributions of direct and indirect photolysis for each QAC are determined. Kinetic studies allow for calculation of second-order reaction rate constants in radical-mediated processes, estimation of quantum yields where relevant, and estimation of environmental half-lives in natural waters.

2. Materials and methods

2.1 Chemicals and reagents

The quaternary ammonium compounds used in this study were: benzyldimethyl-*n*-dodecylammonium chloride (C_{12}-BAC, 98%, Alfa Aesar), benzyldimethyltetradecyl-ammonium chloride hydrate (C_{14}-BAC, 99%, TCI America), benzethonium chloride (BZT, 99%, TCI America), didodecyldimethylammonium bromide (C_{12}-DADMA, 99.9%, Santa Cruz Biotechnology), and didodecyltrimethyl ammonium bromide (C_{12}-ATMA, 99%, Acros Organics). Structures are shown in the ESI Table S1,† and these compounds were selected because they represent high use molecules in different QAC classes. Experimental aqueous stocks, solutions, and buffers were prepared using ultrapure water (resistivity 18.2 MΩ cm, EMD Millipore Corp.). Hydrogen peroxide (H_2O_2, 30%, Fisher) was used as an $^{\bullet}OH$ sensitizer, Rose Bengal (RB, dye content 95%, Sigma-Aldrich) and 2-acetylnaphthalene (2-AN, 99%, Alfa Aesar), were used as $^1O_2$ sensitizers, *para*-chlorobenzoic acid (*p*CBA, 98%, Acros Organics) was used as an $^{\bullet}OH$ probe, furfuryl alcohol (FFA, 98%, Sigma-Aldrich) was used as an $^1O_2$ probe, HPLC grade 2-propanol (IPA, 99.9%, Fisher) was used as an $^{\bullet}OH$ quencher, L-Histidine (His, 99%, Sigma Aldrich) was used as an $^1O_2$ quencher, and sorbic acid (99%, Alfa Aesar) was used as a quenching agent for triplet excited states. *p*-Nitroacetophenone and pyridine (PNAP-PYR) were used as an actinometer.[52,53] Tetraoctylammonium bromide (C_8-TAA, 98%, Sigma Aldrich) and tetrapentylammonium bromide (C_5-TAA, 99%, Sigma Aldrich) were used as internal standards for mass spectrometry analysis. Sodium phosphate monobasic monohydrate (98%, Fisher), sodium phosphate dibasic anhydrous (99%, J.T. Baker), ammonium acetate (97%, Macron), sodium hydroxide (98%, Macron), hydrochloric acid (35%, TraceMetal Grade, Fisher), *o*-phosphoric acid (85%, HPLC Grade, Fisher),

glacial acetic acid (99%, ACS Grade, BDH) and formic acid (88%, ACS Grade, Fisher) were used to prepare buffers for experiments and high-pressure liquid chromatography (HPLC) analysis. HPLC grade methanol (99.9%, Fisher) and HPLC grade acetonitrile (99.9%, Fisher or J.T. Baker) were used as HPLC eluents. Optima LC/MS grade (Fisher Scientific) acetonitrile, water, formic acid, and ammonium acetate were used as eluents for mass spectrometry.

2.2 River water sample collection and analysis

Mississippi River water (MRW) grab samples were collected in Minneapolis, MN in clean (soaked in Alcanox overnight and rinsed 3× with tap water, deionized water, and ultrapure water), combusted (5 hours at 550 °C) Pyrex glass media bottles at Saint Anthony Falls Laboratory (February 27, 2019) and the University of Minnesota Boathouse dock (June 5, 2018). Whole water samples were immediately vacuum filtered through a combusted 0.7 μm glass fiber filter followed by a sterile 0.2 μm Omnipore membrane filter (Millipore) and then stored at 4 °C in the dark prior to photolysis experiments.

River water samples were characterized immediately before conducting photolysis experiments. Nitrate and nitrite were measured by ion chromatography using a Metrohm Compact ion chromatograph model 930. Calibration curves were generated with ACS grade sodium salts and detection limits were 0.1 mg L^{-1} as N for both NO_3^- and NO_2^-. Dissolved organic carbon (DOC), as non-purgeable organic carbon, and dissolved inorganic carbon (DIC) were measured with a Shimadzu TOC-L total organic carbon analyzer. Calibration curves were generated using potassium hydrogen phthalate (≥99.95%, Sigma-Aldrich) for DOC and anhydrous sodium carbonate (ACS grade, Fisher) and sodium bicarbonate (99.7–100.3%, Sigma-Aldrich) for DIC. River water pH was measured using a Thermo Scientific Orion pH probe (calibrated with pH 4, 7, and 10 standard solutions from Fisher). This information is tabulated in Table S2.†

2.3 Absorption spectra

Ultraviolet-visible absorbance of river water as well as aqueous QAC, probe, and actinometer solutions was measured with a Shimadzu UV-1601PC spectrophotometer using 1 cm quartz cuvettes. The light absorption properties of the chemicals are shown in Fig. S1.†

2.4 Analytical methods

Concentrations of QACs with an aromatic group (C_{12}-BAC, C_{14}-BAC, and BZT), the actinometer, and probe compounds were determined by HPLC using an Agilent 1100 LC with a variable wavelength detector. HPLC methods are summarized in Table S3.† C_{12}-DADMA and C_{12}-ATMA were quantified on a Thermo Dionex UltiMate 3000 RSLCnano system equipped with a Thermo TSQ Vantage triple quadrupole tandem mass spectrometer (LC-MS/MS) in positive electrospray ionization mode at the University of Minnesota Masonic Cancer Center using the following parameters: heated electrospray ionization, spray voltage of 2.6 kV, vaporizer temperature of 250 °C, sheath gas pressure of 25 psi, aux gas pressure of 20 psi, capillary temperature of 300 °C, SRM scan width (m/z) of 0.1 and scan time (s) of 0.25. Separation was performed on a Waters XSelect CSH C18 (3.5 μm, 130 Å, 50 × 2.1 mm) column. Flow rate was maintained at 250 μL min^{-1}, sample temperature was 10 °C, the column was kept at room temperature, and 4 μL was injected in the column. Isocratic methods (10 minutes in duration) of mobile phases A: 2 mM ammonium acetate with 0.1% formic acid in water, B: 0.1% formic acid in acetonitrile, and C: isopropanol were used (65% A, 20% B, and 15% C for C_{12}-ATMA and 37% A, 33% B, and 30% C for C_{12}-DADMA). Flow was diverted to waste from 0 to 4.5 minutes. For C_{12}-ATMA the m/z values monitored were 228.26 and 60.15 and the retention time was 6.1 min, and for C_{12}-DADMA they were 382.44, 214.28, and 5.6 min.

2.5 Model sensitizer photochemical experiments

Experiments were performed to determine the reactivity of QACs with $^{\bullet}OH$ using H_2O_2 and with $^1O_2$ using RB and 2-AN. Duplicate experiments were run in sealed quartz test tubes in an Atlas Suntest CPS+ solar simulator equipped with a 1500 W xenon arc lamp and 290 nm cutoff filter, though it has previously been reported that there is some light transmission <290 nm,[49] at a light intensity over 300–800 nm of 765 W m^{-2} for $^{\bullet}OH$ experiments, at 350 W m^{-2} for $^1O_2$ experiments with RB, and at 765 W m^{-2} for $^1O_2$ experiments with 2-AN. The different light intensities were used to control the time over which the reaction occurred. During $^{\bullet}OH$ experiments, QACs (C_{12} and C_{14}-BAC, BZT) and pCBA were spiked from concentrated aqueous stock solutions prepared in unbuffered ultrapure water to achieve an initial concentration of approximately 10 μM in 6–8 mL of phosphate buffer (10 mM, pH 7.0) with 1 mM H_2O_2. Subsamples of 200 or 500 μL were withdrawn at regular time intervals using combusted glass Pasteur pipettes and dispensed into 1.5 mL amber glass HPLC vials with crimp caps. Equivalent experiments with C_{12}-DADMA and C_{12}-ATMA had initial QAC concentrations of 1 μM and a pCBA concentration of 5 μM. Subsamples of 900 μL were dispensed into screw top HPLC vials with 100 μL internal standard mix in acetonitrile (C_8-TAA for C_{12}-DADMA and C_5-TAA for C_{12}-ATMA) for LC-MS/MS analysis and 500 μL samples were withdrawn for pCBA analysis *via* HPLC. Control experiments to account for direct photochemical and non-photochemical losses were performed. Direct controls were run in buffer with the QAC and probe. Dark controls containing the QAC, sensitizer, and probe compound were wrapped in aluminum foil. A quenched control spiked with 1% IPA was also simultaneously run.

Singlet oxygen experiments were conducted in a similar fashion with test tubes containing 8 mL of phosphate buffer (10 mM, pH 7.0), 1–2 μM RB (ground-state reduction potential, $E^o(S/S^-) = -0.54$ V_{SHE}; triplet energy, $E_T = 171$ kJ mol^{-1}; triplet state reduction potential, $E^o{}^*(^3S^*/S^-) = 1.23$ V_{SHE}; $^1O_2$ quantum yield $\Phi_\Delta = 0.75$),[54] 40 μM FFA, and 10 μM BZT or C_{12}-BAC. L-Histidine (20 mM) was used as an $^1O_2$ quencher. To explore the role of $^1O_2$ and triplet states, experiments with deoxygenated (*i.e.*, nitrogen-sparged) solutions were carried out. Additional experiments were conducted for BZT with 16 μM 2-AN (ground-

state reduction potential, E^{o} (S/S^{-}) = −1.48 V_{SHE}; triplet energy, E_T = 249 kJ mol^{-1}; triplet state reduction potential, E^{o}* ($^3S^*/S^{-}$) = 1.10 V_{SHE}; $^1O_2$ quantum yield Φ_Δ = 0.71).[54] Deoxygenated solutions were prepared in an anaerobic glove bag (97% N_2/3% H_2, Pd catalyst, Coy Laboratory Products Inc.) by spiking aqueous stocks (in deoxygenated ultrapure water) of BZT, 2-AN, and FFA in deoxygenated pH7 10 mM phosphate buffer, which was sparged with N_2 gas for 2 hours. The solution was placed into quartz test tubes and further bubbled with N_2 outside of the glove bag for 5–10 minutes prior to being sealed with foil and rubber septa caps. The deoxygenated tubes were sampled sacrificially at 20 and 50 minutes. Another experiment with BZT in deoxygenated phosphate buffer was run with 1 mM sorbic acid to quench triplets.[55,56] Sorbic acid was stirred overnight on a heated stir plate and then sonicated and degassed with application of vacuum for 10–20 minutes at 30–40 °C before being brought into the glove bag. Other solutions were prepared as above, and all sample solutions were bubbled with N_2 outside the glove bag for 30 minutes prior to being dispensed into test tubes under a nitrogen blanket and sealed with foil and rubber septa caps. Tubes were sampled sacrificially after 10, 20, 30, 40, and 50 minutes.

Steady-state concentrations of hydroxyl radicals ($[^{\bullet}OH]_{ss}$) and singlet oxygen ($[^1O_2]_{ss}$ were calculated from the ratio of the measured pseudo-first-order rate constant (k_{obs}), determined *via* linear regression, and the bimolecular reaction rate constant of *p*CBA with $^{\bullet}OH$ ($k_{^{\bullet}OH,pCBA} = 5 \times 10^9$ M^{-1} s^{-1})[57] and FFA with $^1O_2$ ($k_{^1O_2} = 1.17 \times 10^8$ M^{-1} s^{-1} at 30 °C).[58] Direct photolysis losses of the probes were negligible. Assuming a first-order kinetic dependence on each QAC and *p*CBA and that the reactions proceed independently, bimolecular reaction rate constants of QACs with $^{\bullet}OH$ ($k_{^{\bullet}OH,QAC}$) were derived using competition kinetics according to eqn (1).

$$\ln\left(\frac{[QAC]}{[QAC_0]}\right) = \ln\left(\frac{[pCBA]}{[pCBA_0]}\right)\frac{k_{^{\bullet}OH,QAC}}{k_{^{\bullet}OH,pCBA}} \quad (1)$$

The rate constants for the respective QACs were obtained from linear regressions of logarithmic plots of normalized QAC *versus* *p*CBA concentrations in the same tube.

2.6 Simulated and outdoor photochemical experiments in river water

QAC photolysis experiments were performed on Mississippi River water and phosphate buffer under simulated and natural sunlight to assess the relative importance of direct photolysis and indirect photochemical transformation due to PPRIs. The radical-specific probe *p*CBA was used for the quantification of $^{\bullet}OH$ steady-state concentrations in the same tube. Direct photolysis controls were performed for all QACs and *p*CBA in phosphate buffer solutions (10 mM, pH 7.0), and dark control experiments for QACs and *p*CBA in river water were performed in tubes wrapped with aluminum foil. River water solutions spiked with 1% IPA as a radical quencher were concurrently irradiated to evaluate the importance of indirect photolysis processes involving $^{\bullet}OH$. Time resolved samples of 200 or 500 μL were removed for HPLC analysis to determine reaction kinetics.

For simulated sunlight experiments, C_{12} and C_{14}-BAC and BZT were photolyzed in filtered Mississippi River water using a solar simulator. The light intensity was set to 765 W m^{-2}, and samples were taken every 5 hours. All experiments were run in duplicate. For outdoor natural sunlight experiments, C_{12} and C_{14}-BAC and BZT were photolyzed in filtered Mississippi River water collected on June 5, 2018 over a total of 26.8 hours from June 28, 2018 to July 6, 2018 (Table S4† summarizes the exposures) on the rooftop of the University of Minnesota Mechanical Engineering building (latitude: 44°58′30″N, longitude: 93°14′1″W, elevation: 860 ft, azimuth: 218°SW).

Aliquots of 6–8 mL initial volume reaction solutions in 10 mL quartz test tubes (13 mm o.d. and 11 mm i.d.) were sealed with pre-combusted aluminum foil squares and then rubber septa caps. The test tubes were irradiated at a 30° angle from the horizontal. Initial QAC and probe concentrations were nominally 10 μM, allowing for direct monitoring of reactant and probe compound concentrations and minimization of light screening.

The chemical actinometer PNAP-PYR was simultaneously irradiated during simulated and natural sunlight river water experiments to estimate the spectral irradiance of the light source, calculate direct photolysis quantum yields for QACs at low optical density, and plot long duration experimental data by dose *via* actinometer loss to compare laboratory and outdoor experiments. The PNAP-PYR actinometer was chosen because the half-life of the QACs was expected to be greater than 4 hours based on preliminary experiments. The concentrations of pyridine were set using relationships in Leifer[52] such that the actinometer loss rate would occur over the same time scale as the QAC loss. The spectral irradiance of the solar simulator at wavelengths 276–400 nm was estimated using a bimolecular solution of 47.2 mM pyridine added to 10.7 μM *p*-nitroacetophenone for a desired half-life of 17 hours in river water experiments. For rooftop experiments, a 11.4 μM PNAP/52.3 mM pyridine solution was used. The molar absorptivity of PNAP (ε_{PNAP}) was calculated by linear regression of absorbance measurements of 3 analytical standards (concentrations 5, 10, and 15 μM) prepared in Milli-Q with trace acetonitrile.

The SMARTS 2.9.5 model[59–61] was used to calculate the solar spectral irradiance (Fig. S1†) over the time course of outdoor experiments. Salient inputs are summarized in ESI Table S5.† Global tilted irradiances were calculated for each solar hour in an experimental day, summed, and divided by the total exposure hours for each day. The daily irradiances were then averaged for quantum yield calculations.

Direct photolysis quantum yields were calculated following the methods outlined in Dulin and Mill[53] and Leifer[52] with the updated PNAP-PYR quantum yield relationship published by Laszakovits *et al.*,[62] summarized by eqn (2).

$$\phi_{dc} = \frac{k_{dc}}{k_{da}}\frac{\sum_\lambda (I_\lambda \varepsilon_{\lambda a})}{\sum_\lambda (I_\lambda \varepsilon_{\lambda c})}\phi_{da} \quad (2)$$

I_λ = the irradiance (intensity) of incident light in einsteins m^{-2} s^{-1} at a fixed wavelength λ. ε_λ = the decadic molar absorption coefficient of the actinometer (a) or the compound (c) in M^{-1} m^{-1}. The molar absorptivity of the QAC cation was determined by measuring the absorption spectra of a 100 μM solution in buffer and subtracting the absorption of an equivalent concentration of the counter anion (100 μM NaCl or NaBr) as a blank. $\phi_{da} = \phi_{PNAP} = 0.0074[pyr] + 1.1 \times 10^{-5}$.[62] $\frac{k_{dc}}{k_{da}}$ = the slope of the logarithmic plot of direct photodegradation of the compound *versus* actinometer determined by linear regression. The wavelength range was 276 to 400 nm for the solar simulator and 280 to 400 nm for outdoor experiments.

2.7 Data analysis

Data points from replicate experiments were plotted individually. The slope of the regression lines and their standard error were used to calculate the required slopes/reaction rate constants and the associated 95% confidence intervals, respectively. Linear fits and generation of rate constants, standard errors of slopes, and 95% confidence intervals were performed with Origin, Version 2017 (OriginLab Corporation, Northampton, MA, USA).

3. Results and discussion

3.1 Reactivity of QACs with ˙OH from H_2O_2 sensitizer experiments

Based on previous work with ionic liquids,[63] ˙OH was hypothesized to be an important PPRI for the indirect photochemical transformation of QACs. Competition kinetics experiments were conducted with H_2O_2 and *p*CBA to determine bimolecular reaction rate constants between QACs and ˙OH ($k_{\cdot OH,QAC}$). Fig. 1 shows the natural log of the ratio of concentration normalized by the initial concentration of QACs during a solar simulator irradiation experiment with H_2O_2 producing ˙OH. The C_{12}-ATMA H_2O_2 40 minute data points (Fig. 1D) were treated as outliers due to anomalous instrumental measurements, indicated by open symbols, and excluded from the ensuing regression and analysis. For all the compounds studied, photolysis in the presence of ˙OH follows pseudo-first order kinetics ($r^2 \geq 0.83$). Dark controls dosed with H_2O_2 showed no significant change in QAC concentration. Quantification of steady-state ˙OH concentrations was done using *p*CBA (Fig. S2 and Table S6†).

Fig. 2 shows the log–log plot of concentrations of the 5 QACs *versus* that of *p*CBA. Using the slopes of the linear regressions in Fig. 2 and the bimolecular reaction rate constant of *p*CBA with ˙OH, $k_{\cdot OH,QAC}$ values were calculated for the QACs using eqn (1) (Table 1).

The results demonstrate that the QACs studied react with ˙OH at or near the diffusion-controlled limit (*i.e.*, $k_{\cdot OH,c} = 5 \times 10^9 - 10^{10}$ M^{-1} s^{-1}), which is the case for many organic contaminants.[57,64] The hydroxyl radical reacts unselectively with most organic compounds and reactions occur at different functional groups. Typically, ˙OH behaves as an electrophile and reacts with organic pollutants in two ways: (1) OH group addition to an aromatic ring or a double bond and (2) hydrogen atom abstraction from aliphatic carbon-hydrogen bonds.[57,64] The structural differences of the studied QACs did not significantly affect the bimolecular rate constant, except the reaction between DADMA and ˙OH is about an order of magnitude lower than for the other compounds.

Similar to imidazolium cations,[63] there was a slight trend seen for increasing $k_{\cdot OH,QAC}$ with the increasing side chain length of C_{12} and C_{14}-BAC though the values are within error. For C_{12}-DADMA, where reaction with ˙OH only occurs *via* H atom abstraction at C–H bonds in the side chains, rates were smaller than for BACs and BZT, and C_{12}-ATMA. The exchange of a methyl group (ATMA) for a 12 carbon alkyl chain (DADMA) noticeably slows the reaction kinetics. The alkoxy groups in BZT have both inductive electron withdrawing and resonance electron-donating effects. The hydroxyl radical reacts rapidly with compounds containing aromatic rings with electron-donating substituents, and addition reactions still occur at appreciable rates in the presence of electron-withdrawing groups.[64] The coincidence in rates for the BACs, BZT, and C_{12}-ATMA suggests that H atom abstraction at C–H bonds in the side chain contributes to the overall reaction of BACs and BZT with ˙OH in addition to any reaction at the ring.

3.2 Assessing reactivity with other PPRIs

To further explore the role of specific PPRIs in QAC degradation in the presence of DOM and more definitively rule out additional pathways, sensitizer experiments were conducted to assess reactivity with $^1O_2$ and triplet excited states. Because $^1O_2$ is a selective electrophile preferentially reacting with electron-rich functional groups like sulfides, phenols, alkenes and aromatic compounds, anilines, furans, and other electron-rich heterocycles,[58,65,66] it was hypothesized QACs would have limited interaction with this reactive oxygen species. Moreover, because DOM can be a microheterogeneous environment in which $^1O_2$ potentially reaches higher steady-state concentrations[51,67] and QACs will associate with DOM, enhanced reactivity might occur if in fact they do react with $^1O_2$.

Experiments with RB showed no reaction between C_{12}-BAC (Fig. S3A†) and $^1O_2$ (FFA was used to measure the bulk concentration of $^1O_2 - [^1O_2]_{ss} = (3.9 \pm 1.2) \times 10^{-12}$ M) (Fig. S3B, Table S7†) under air saturated conditions, and there was no statistically significant difference between the pseudo-first-order rate constant for C_{12}-BAC loss with RB and the histidine quenched and dark controls. No loss of C_{12}-BAC was observed in the deoxygenated control as well, indicating no reactivity with triplet excited states of RB.

BZT exhibited possible reactivity with the triplet excited state of RB based on decay in the histidine quenched control, and BZT loss in the dark control suggested that BZT was also potentially reacting with RB (Fig. S4†). Additional control experiments (not shown) indicated that BZT interacts with RB under ambient, dark conditions and therefore a different $^1O_2$ sensitizer, 2-AN, which is also a model ^{3}DOM* sensitizer, was used.

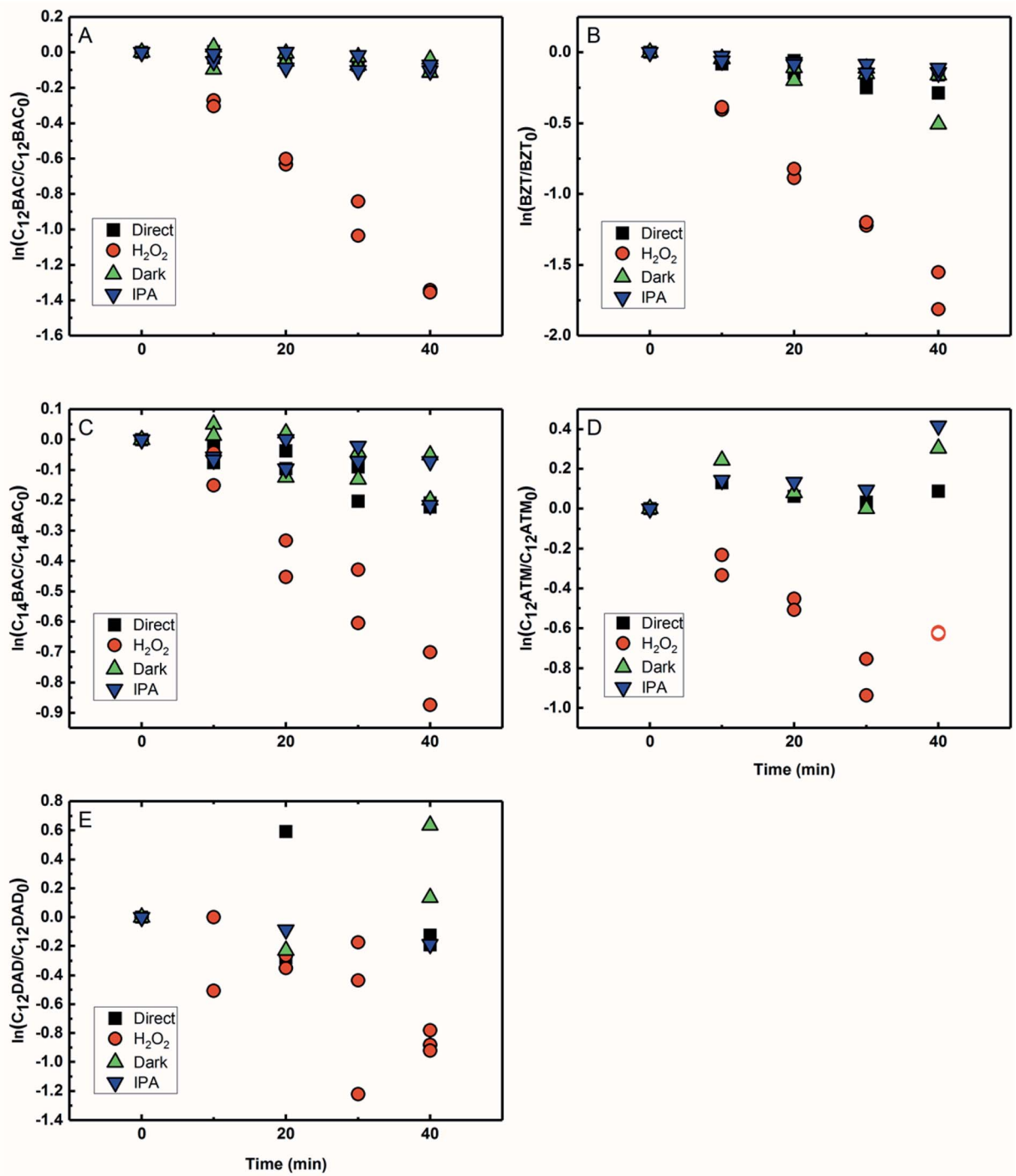

Fig. 1 Phototransformation over time of: C_{12}-BAC (A), BZT (B), C_{14}-BAC (C), C_{12}-ATMA (D), and C_{12}-DADMA (E) in the presence of *p*CBA under simulated sunlight in phosphate buffer (direct, black squares), with 1 mM hydrogen peroxide (H_2O_2, red circles), H_2O_2 dark control (dark, green triangle), and H_2O_2 with 1% isopropanol (IPA, blue upside down triangle). Open symbols denote outliers.

The experiments with BZT and 2-AN illustrated minimal BZT loss due to $^1O_2$ (Fig. S5A†), and there was no statistically significant difference between the 2-AN results and the dark control and the histidine control where $^1O_2$ is quenched. A deoxygenated control experiment was also conducted. Interestingly, in the deoxygenated solution containing 2-AN, BZT exhibited an approximately 84% decrease after 50 minutes of irradiation. The addition of sorbic acid, which quenches triplet-excited states (with energy >200 kJ mol^{-1}) of organic compounds, to the deoxygenated 2-AN solution slowed the reaction by 95%. These results indicate that BZT reacts with ^{3}2-AN*. FFA also reacted in the presence of 2-AN, but degassing the 2-AN solution resulted in a 23% decrease in the pseudo-first-order rate constant of FFA compared to FFA in an air-saturated

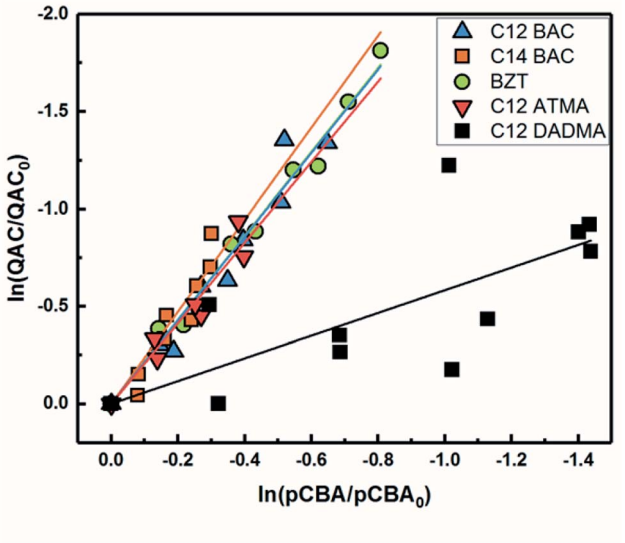

Fig. 2 log–log concentrations of QACs *versus para*-chlorobenzoic acid from solar simulator irradiation experiments with hydrogen peroxide. Solid lines represent linear regressions.

solution (Fig. S5B†), indicating a role for both $^1O_2$ and ^{3}2-AN*. Furthermore, minimal loss of FFA was observed in the deoxygenated solution upon addition of sorbic acid, reiterating that FFA is susceptible to degradation by organic triplets.[68,69] Together, these results indicate that BZT does react with ^{3}2-AN*, but the reaction only occurs in the absence of oxygen, meaning quenching of the triplets by oxygen is faster than the reaction with BZT. Thus, BZT reaction with triplet excited state organic matter will likely be unimportant in environmental systems because dissolved oxygen in surface waters will efficiently scavenge triplets before they react with BZT.

3.3 Photochemical transformation of BACs in river water under simulated and natural sunlight

The transformation of BACs was then investigated in the presence of DOM in river water. Based on their chemical structures, no other processes besides reactivity with $^{\bullet}$OH would occur to transform ATMA and DADMA, and further experiments were not conducted in river water. Fig. 3A and B show the time course of C_{12}-BAC and C_{14}-BAC concentrations in phosphate buffer and Mississippi River water in the solar simulator. The tubes were irradiated for a total of 30 hours and this exposure was almost continuous with tubes being removed after 5 or 10 hour increments for sampling and then being returned to resume irradiation in the solar simulator. The loss in river water exhibits pseudo-first-order kinetics as attested to by logarithmic plots for QAC photolysis *versus* actinometer loss (Fig. S6†). To evaluate the oxidation of BACs by $^{\bullet}$OH, the probe *p*CBA was added to each MRW tube with BAC, allowing for competition kinetics and quantification of $[^{\bullet}OH]_{ss}$.

For C_{12}-BAC, 9% loss of the compound was seen in the direct photolysis control and 4% in the IPA quenched control. No apparent loss was exhibited in the dark control; in fact, a slight increase was observed possibly due to evaporation or variation in analytical reproducibility. The slopes for the direct ($k_{direct} = (2 \pm 1) \times 10^{-3}$ h^{-1}) and IPA quenched ($k_{IPA} = (1.7 \pm 0.3) \times 10^{-3}$ h^{-1}) controls were within error. Estimating an indirect pseudo-first-order rate constant from the bimolecular reaction rate constant determined from H_2O_2 sensitizer experiments and the calculated $[^{\bullet}OH]_{ss}$ from *p*CBA loss in MRW (Table 1) gives (2.7 ± 0.3) $\times$ 10^{-2} h^{-1}, which is nearly identical to the overall rate constant for C_{12}-BAC degradation in MRW ($(2.9 \pm 0.4) \times 10^{-2}$ h^{-1} (Table S8†)), reaffirming that the loss seen in the MRW is due to the reaction with $^{\bullet}$OH.

For C_{14}-BAC, a slight increase was observed in the direct control possibly from evaporation in the solar simulator or instrumental error in the measurements. The data in the direct, dark, and IPA quenched controls had consistent trends from 5 to 30 hours. While C_{14}-BAC exhibited an average 14% and 18% decrease from the initial concentration in the dark and IPA quenched controls, respectively, the slopes ($k_{dark} = (3 \pm 3) \times 10^{-3}$ h^{-1} and $k_{IPA} = (5 \pm 3) \times 10^{-3}$ h^{-1}) demonstrate negligible depletion in these controls compared to the loss in MRW. The overall rate constant for C_{14}-BAC degradation in MRW was $k_{MRW} = (2.8 \pm 0.6) \times 10^{-2}$ h^{-1}, which agrees with the estimated pseudo-first-order reaction rate constant for C_{14}-BAC loss due to the reaction with $^{\bullet}$OH ($(2.9 \pm 0.4) \times 10^{-2}$ h^{-1}).

Photolysis proceeded faster in the presence of dissolved organic matter, indicating the importance of indirect photolysis (Table S8†). The addition of the radical inhibitor IPA reduced the photodegradation rates substantially in MRW for C_{12} $\left(\frac{k_{IPA}}{k_{MRW}} = (6 \pm 1) \times 10^{-2}\right)$ and C_{14}-

Table 1 Bimolecular reaction rate constants of QACs with hydroxyl radicals, $k_{^{\bullet}OH,QAC}$ (M^{-1} s^{-1}), determined using hydrogen peroxide as a sensitizer as well as those determined in Mississippi River water under simulated and natural sunlight[a]

	Hydrogen peroxide	Solar simulator, river water		Outdoors, river water	
QAC	$k_{^{\bullet}OH,QAC}$ (M^{-1} s^{-1})	$[^{\bullet}OH]_{ss}$ (M)	$k_{^{\bullet}OH,QAC}$ (M^{-1} s^{-1})	$[^{\bullet}OH]_{ss}$ (M)	$k_{^{\bullet}OH,QAC}$ (M^{-1} s^{-1})
C_{12}-BAC	$(1.1 \pm 0.1) \times 10^{10}$	$(7.0 \pm 0.2) \times 10^{-16}$	$(1.1 \pm 0.2) \times 10^{10}$	$(3.8 \pm 0.3) \times 10^{-16}$	$(1.2 \pm 0.1) \times 10^{10}$
C_{14}-BAC	$(1.2 \pm 0.2) \times 10^{10}$	$(6.7 \pm 0.1) \times 10^{-16}$	$(1.2 \pm 0.3) \times 10^{10}$	$(3.8 \pm 0.3) \times 10^{-16}$	$(1.2 \pm 0.3) \times 10^{10}$
BZT	$(1.08 \pm 0.05) \times 10^{10}$	$(6.1 \pm 0.4) \times 10^{-16}$	$(9.3 \pm 1.3) \times 10^{9}$	$(3.9 \pm 0.4) \times 10^{-16}$	$(9.4 \pm 3.2) \times 10^{9}$
C_{12}-ATMA	$(1.03 \pm 0.14) \times 10^{10}$				
C_{12}-DADMA	$(2.9 \pm 1.0) \times 10^{9}$				

[a] Errors represent 95% confidence intervals associated with the regression slopes in Fig. 2.

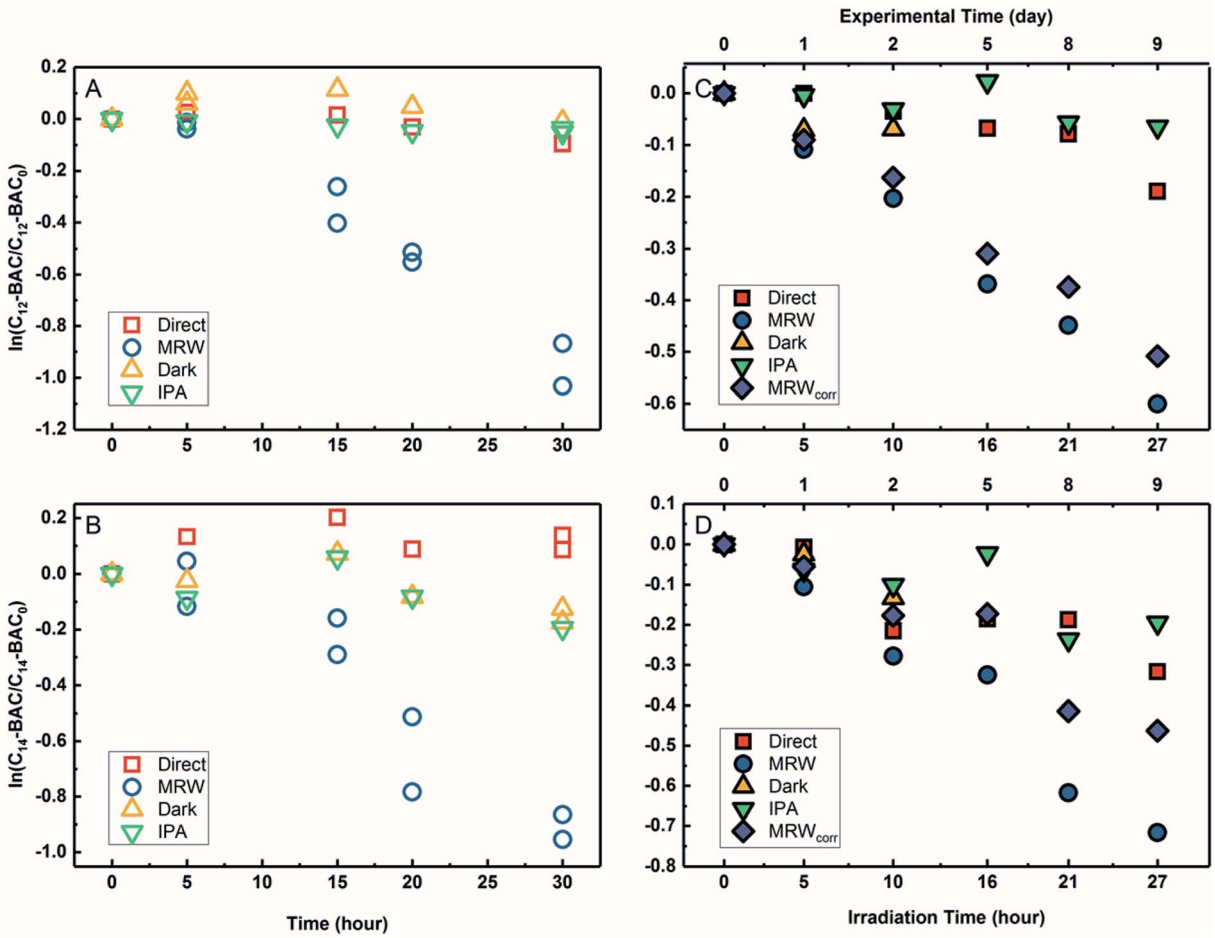

Fig. 3 Photolysis of BACs with *p*CBA under simulated sunlight (C_{12}: A, C_{14}: B) or natural sunlight (C_{12}: C, C_{14}: D) in phosphate buffer (direct, red squares), Mississippi River water (MRW, blue circles), MRW dark control (yellow triangle), and MRW with 1% isopropanol (IPA, green upside down triangle). Indirect photochemical loss in river water is shown by purple diamonds (MRW_{corr}). Note the top *x*-axis for outdoor plots C and D showing the total duration of the experiment.

BAC $\left(\frac{k_{IPA}}{k_{MRW}} = (1.6 \pm 1.0) \times 10^{-2}\right)$. The quencher results demonstrate that direct photochemical loss of BACs is likely to be relatively unimportant in natural systems and indicate that the $^{\bullet}OH$ produced is responsible for BAC loss.

Analogous outdoor experiments were conducted in river water to verify the transferability of indoor photolysis results for the BACs. Fig. 3C and D show the time course of C_{12}-BAC and C_{14}-BAC concentrations in phosphate buffer and Mississippi River water in natural sunlight. Logarithmic plots of BAC *versus* actinometer loss (Fig. S7†) indicate that outdoor photolysis also follows pseudo-first-order kinetics. *p*CBA was again added to MRW tubes.

The overall rate constant for C_{12}-BAC degradation in MRW in natural sunlight was $(2.2 \pm 0.1) \times 10^{-2}$ h^{-1}. Estimating an indirect pseudo-first-order rate constant from the bimolecular reaction rate constant determined from H_2O_2 sensitizer and solar simulator river water experiments and the calculated $[^{\bullet}OH]_{ss}$ from *p*CBA loss in MRW (Table 1) gives $(1.5 \pm 0.1) \times 10^{-2}$ h^{-1} and $(1.5 \pm 0.3) \times 10^{-2}$ h^{-1}, respectively. These estimates imply that 67 to 71% of C_{12}-BAC loss in MRW in the outdoor experiment could be attributable to the reaction with $^{\bullet}OH$. IPA suppressed the reaction in river water substantially ($k_{IPA}/k_{MRW} = (8 \pm 8) \times 10^{-2}$).

For C_{14}-BAC, the overall rate constant in MRW was $k_{MRW} = (2.6 \pm 0.4) \times 10^{-2}$ h^{-1}. The indirect pseudo-first-order rate constant estimates ($(1.6 \pm 0.3) \times 10^{-2}$ h^{-1} from H_2O_2 sensitizer and $(1.6 \pm 0.4) \times 10^{-2}$ h^{-1} from solar simulator river water experiments) suggest that 61 to 62% of C_{14}-BAC loss in MRW in the outdoor experiment could be attributable to the reaction with $^{\bullet}OH$. IPA suppressed the reaction in river water, though not completely $\left(\frac{k_{IPA}}{k_{MRW}} = (3 \pm 2) \times 10^{-1}\right)$. At the end of the experiment, about an 18% decrease in C_{14}-BAC concentration was seen in the quenched control and 27% in the direct control, though these losses are relatively minor compared to the losses in MRW over the same time period.

Because the overlap between the absorption spectra of the BACs and the solar spectrum is small, direct photochemical loss is slow and DOM might screen light affecting transformation rates. Additionally, BACs are hydrolytically stable. Though all C_{12}-BAC control slopes are relatively rather small and associated

with proportionate error ($k_{direct} = (6 \pm 2) \times 10^{-3}$ h^{-1}, $k_{IPA} = (2 \pm 2) \times 10^{-3}$ h^{-1}, and $k_{dark} = (8 \pm 9) \times 10^{-3}$ h^{-1}), a slight loss seems to be occurring in the MRW outdoors due to other abiotic and/or biotic mechanisms. The losses in C_{14}-BAC are more pronounced. Slight thermal decay due to elevated temperatures outside, sorption to the walls of the test tube over the outdoor exposure period, and/or biodegradation could be occurring concomitantly with indirect photolysis to account for increased degradation in the controls.

Outdoor experiments took approximately 9 days while solar exposure time was a little over a day in total to account for weather and sunshine hours on the rooftop. While the river water was filter-sterilized prior to use in experiments and test tubes were capped, no special protocols were used to maintain sterile conditions for the entirety of the experiment. Therefore, it cannot be ruled out that the difference in predicted rate constants due to $^{\bullet}$OH and the observed rate constant is due to biodegradation because BACs are known to be susceptible to aerobic biodegradation.[32–35,70]

The outdoor river water (MRW) rates were thusly corrected for concentration changes in the controls by eqn (3).[71] The indirect losses were plotted separately (MRW_{corr} in Fig. 3C and D), and the pseudo-first-order rate constants from MRW_{corr} were used to calculate bimolecular reaction rate constants with $^{\bullet}$OH in the outdoor experiments (see below).

$$MRW_{corr}(t) = MRW(t)e^{(-k_{obs,control} \times t)} \quad (3)$$

3.4 BZT direct photolysis in river water under simulated and natural light

The degradation of BZT in MRW appeared to be a combination of direct and indirect photolysis (Fig. 4A) in the solar simulator. Correcting the BZT concentration measured in MRW to account for the loss due to direct photolysis using eqn (3) allowed for calculation of the indirect photolysis pseudo-first-order rate constant and for competition kinetics calculations. The indirect photolysis of BZT in river water is shown in Fig. 4 by the plotted MRW_{corr} data. The probe *p*CBA was used to evaluate the oxidation of BZT by $^{\bullet}$OH, by addition to each MRW tube with BZT, allowing for competition kinetics and quantification of $[^{\bullet}OH]_{ss}$.

The BZT direct photolysis quantum yield from solar simulator experiments was determined using eqn (2) and the photon fluence of the solar simulator determined from actinometry and the photon irradiance provided by the manufacturer (spectral flux, $I^0 = 5.4$ Es L^{-1} s^{-1}). Fig. S8† shows the logarithmic plot of BZT direct photolysis (from both the IPA quenched and direct controls) *versus* the PNAP actinometer. The slope of the line determined by linear regression (1.18 for IPA *vs.* PNAP and 1.11 for direct *vs.* PNAP) was used to calculate quantum yields. $\Phi_{BZT,indoor,IPA}$ was determined to be 6.3×10^{-2} (mol Ei^{-1}) while $\Phi_{BZT,indoor,direct}$ was 5.9×10^{-2} (mol Ei^{-1}). There is good agreement between the two estimates, demonstrating that the decrease of BZT seen in the IPA quenched control is due to direct photolysis and not any other process.

Outdoor experiments were carried out to compare data generated under simulated sunlight with those generated under natural sunlight and to verify the BZT quantum yield obtained in the laboratory because quantum yield calculations are sensitive to irradiance values. For BZT sunlight experiments (Fig. 4B), BZT loss exhibited pseudo-first-order kinetics in river water as seen in the logarithmic plots for QAC photolysis *versus* actinometer loss (Fig. S7†). As with the solar simulator experiment, *p*CBA was simultaneously irradiated in the MRW tubes.

The slopes of linear regressions for the BZT quenched and direct photolysis controls were identical within error due to overlapping confidence intervals. The data points were

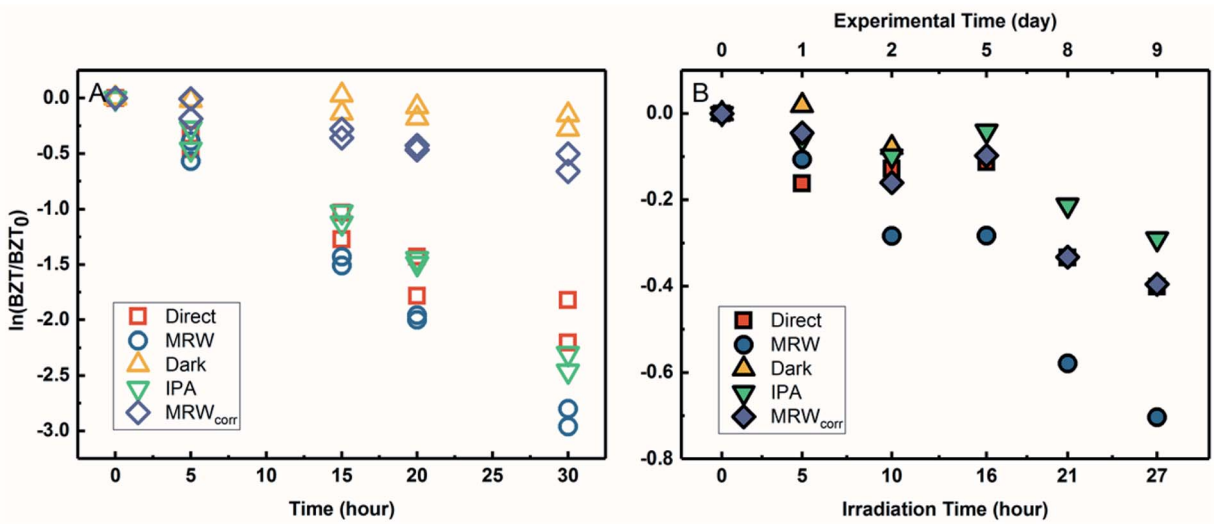

Fig. 4 Photolysis of BZT with *p*CBA under simulated sunlight (A) or natural sunlight (B) in phosphate buffer (direct, red squares), Mississippi River water (MRW, blue circles), MRW dark control (yellow triangle), and MRW with 1% isopropanol (IPA, green upside down triangle). Indirect photochemical loss in river water is shown by purple diamonds (MRW_{corr}). Note the top *x*-axis for outdoor plot B showing the total duration of the experiment.

subsequently combined and fitted using a linear fit of concatenated data in Fig. S8,† which shows the logarithmic plot of BZT direct photolysis *versus* actinometer loss. The direct photolysis quantum yield, $\Phi_{BZT,outdoor}$, was determined to be 1.7×10^{-2} (mol Ei^{-1}) using eqn (2), the slope of 0.21 from Fig. S8,† and the average global tilted irradiance over the timecourse of the rooftop exposures from SMARTS. The discrepancy in calculated quantum yields and half-lives can be explained by the fact that, as has been reported previously,[49] though the Xe lamp has a filter that prevents the transmission of wavelengths below 290 nm, there is a bleed of wavelengths <290 nm, which introduces systematic error. This error is important for QACs like BZT which absorb weakly above 290 nm and thus direct photolysis rates are over-emphasized.[72] In the terrestrial aquatic environment, direct photolysis occurs for chemicals that absorb photons at wavelengths ≥290 nm because the upper atmosphere screens out solar irradiance at shorter wavelengths. Despite errors introduced by the solar simulator and differences in quantum yields due to spectral overlap, direct photolysis of BZT would still occur in the environment, but the quantum yield determined in sunlight should be used in the calculation of predicted half-life.

3.5 Second-order rate constants with ˙OH in river water

Because *p*CBA was included in the river water experiments, competition kinetics can be used to determine the second order rate constant with ˙OH to test for any effect of the matrix or light source by comparing the results to those measured with H_2O_2. Fig. 5 shows the competitive oxidation of the QACs by ˙OH in MRW under simulated and natural sunlight corrected for losses not due to indirect photolysis. As with the ˙OH sensitizer experiments, BZT, C_{12}-BAC, and C_{14}-BAC react with ˙OH in the river water at or near diffusion controlled rates. Association with dissolved organic matter did not significantly influence the photochemical transformation rates of QACs with ˙OH based on the similarity of the values (within 10%) to those determined using H_2O_2 as a sensitizer.

The outdoor experimental data overlay the indoor results in river water demonstrating that simulated sunlight experiments serve as good proxies for understanding the photochemical behavior of QACs in surface waters with respect to reaction with ˙OH. All calculated bimolecular reaction rate constants (Table 1) are within the 95% confidence intervals for the 3 sets of experiments serving as robust validation of the values. Due to the overlap of the indoor and outdoor results, we can be reasonably assured in our assumptions about the outdoor experimental data and that the indirect photolysis estimates are correct. Fig. 5 reaffirms that the photochemical fate of QACs in the environment will be highly dependent on ˙OH generation in natural waters.

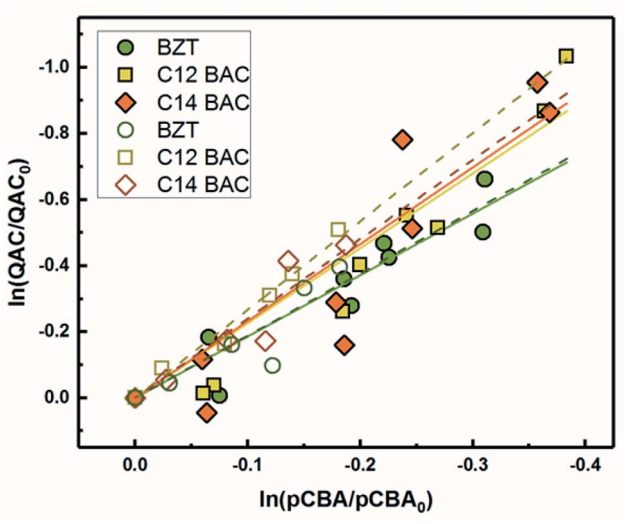

Fig. 5 log-concentrations of QACs *versus para*-chlorobenzoic acid from solar simulator (solid symbols) and natural sunlight (open symbols) irradiation experiments in MRW. QAC concentrations are corrected to only reflect indirect photochemical loss due to ˙OH. Solid and dashed lines represent linear regressions for solar simulator and natural sunlight experiments, respectively.

3.6 Calculated half-lives in surface waters

The relative contributions of indirect and direct photolysis were evaluated by comparison of pseudo-first-order rate constants from experiments with river and ultrapure water under simulated and natural sunlight. For most of the QACs studied, direct photolysis under environmental conditions is either slow or nonexistent. Only BZT exhibited appreciable direct photochemical degradation. Direct photolysis half-lives for BZT were estimated to be 5.4–5.7 days under simulated sunlight and 20.6 days in natural sunlight using a direct photolysis rate constant calculated using the solar spectra modeled by SMARTS (Fig. S1†). While the reaction between QACs and ˙OH is diffusion controlled, QAC degradation *via* this process will be relatively slow in the environment. The bimolecular reaction rate constants with ˙OH were used to estimate half-lives of the tested QACs in sunlit surface waters using eqn (4) and assuming an $[^{\bullet}OH]_{ss}$ of 1×10^{-16} M on average over 7 hours of daily sunshine.[63] Maximum near-surface steady-state ˙OH concentrations range from 10^{-17} to 10^{-15} M in sunlit surface waters depending on the concentrations of photoproducing and scavenging species, latitude, and time of year.[64,73,74] The half-lives of QACs in the photic zone presented in Table 2 reflect a lower bound (minimum persistence) because they are estimated based on conditions in which average maximum rates of ˙OH photoproduction occur in the photic zone of a water body at midday during the summertime.

$$t_{1/2} = \frac{\ln(2)}{k_{^{\bullet}OH,QAC} \times [^{\bullet}OH]_{ss}} \quad (4)$$

Because BZT is susceptible to both indirect and direct photolysis under relevant environmental conditions, the half-life of BZT in river water is estimated by extrapolating the experimental results for BZT and using the overall pseudo-first-order rate constant for photolytic loss (eqn (5)), where k_c (ESI S3 eqn (1)†) is the direct photolysis pseudo-first-order rate constant of BZT in river water under natural sunlight.

Table 2 Estimated QAC half-lives in surface water in H_2O_2 sensitizer, simulated sunlight (indoor) river water, and natural sunlight (outdoor) river water experiments[a,b]

QAC	$t_{1/2}$ (days) H_2O_2	$t_{1/2}$ (days)[c] river water indoor	$t_{1/2}$ (days)[c] river water outdoor
C_{12}-BAC	26 ± 2	24 ± 4	24 ± 2
C_{14}-BAC	23 ± 3	24 ± 5	23 ± 6
BZT	26 ± 1	12 ± 1	12 ± 2
ATMA	27 ± 4		
DADMA	94 ± 32		

[a] Errors represent 95% confidence intervals. [b] Calculated assuming 7 hours of sunshine per day. [c] BZT $t_{1/2}$ including direct photolysis + $^{\bullet}OH$.

$$k_{obs,BZT} = k_{^{\bullet}OH,BZT} \times [^{\bullet}OH]_{ss} + k_c \quad (5)$$

While QACs demonstrate shorter lifetimes compared to ionic liquid cations,[63] they still have half-lives on the order of weeks to months, highlighting their slow photochemical transformation in rivers and lakes, and their persistence in the aquatic environment. The results and half-life estimates were consistent for outdoor and indoor river water photolysis experiments as well as for H_2O_2 sensitizer experiments, reiterating the importance of $^{\bullet}OH$ over other PPRIs in the fate of QACs in surface waters.

4. Conclusions

The current study elucidates the photochemical fate of QACs in surface waters. For most of the QACs evaluated, indirect photolysis is more important than direct photolysis under simulated and natural sunlight. Through model sensitizer and quencher experiments, it is clear that all QACs studied will react predominantly with $^{\bullet}OH$ produced in natural waters despite variations in structure, such as side-chain length and presence of aromatic rings. In waters with low steady-state $^{\bullet}OH$ concentrations and deeper in the water column, the rates of reaction between QACs and $^{\bullet}OH$ will be substantially slower and thus QAC lifetimes will be longer. The results of this study contribute to a more holistic and systematic evaluation of the fate of QACs in near-surface waters as well as the potential for their attenuation in the environment. Reported half-lives and rate constants can be used in future models to predict the fate of QACs in the environment, which could inform risk assessments and regulatory decisions on biocide usage given the growing public health concern over the proliferation of antibiotic resistant bacteria in the environment. Additionally, the hydroxyl radical reaction data could be applied to assessing the removal of QACs during advanced oxidation treatment.

Conflicts of interest

The authors declare no conflicts of interest.

Acknowledgements

We would like to acknowledge Dr Sarah Pati for help with LC-MS/MS measurements as well as Makenzie Pillsbury. Mass spectrometry was carried out in the Analytical Biochemistry Shared Resources of the Masonic Cancer Center, University of Minnesota, funded in part by Cancer Center Support Grant CA-77598. The authors thank Annika Heaps and Bryanna Lopez-Moran for assistance with laboratory work. This work was funded by the Minnesota Environmental and Natural Resources Trust fund (M.L. 2017, Chp. 96, Sec. 2, Subd. 04a) as recommended by the Legislative and Citizen Commission on Minnesota Resources.

References

1 C. Zhang, F. Cui, G. Zeng, M. Jiang, Z. Yang, Z. Yu, M. Zhu and L. Shen, Quaternary ammonium compounds (QACs): a review on occurrence, fate and toxicity in the environment, *Sci. Total Environ.*, 2015, **518–519**, 352–362.
2 G.-G. Ying, Fate, behavior and effects of surfactants and their degradation products in the environment, *Environ. Int.*, 2006, **32**, 417–431.
3 U. Tezel and S. G. Pavlostathis, Role of Quaternary Ammonium Compounds on Antimicrobial Resistance in the Environment in *Antimicrobial Resistance in the Environment*, John Wiley & Sons, Inc., Hoboken, NJ, USA, 2011, pp. 349–387.
4 M. T. García, E. Campos, J. Sanchez-Leal and I. Ribosa, Effect of the alkyl chain length on the anaerobic biodegradability and toxicity of quaternary ammonium based surfactants, *Chemosphere*, 1999, **38**, 3473–3483.
5 J. Hong, U. Tezel, D. Okutman Tas and S. G. Pavlostathis, Influence of quaternary ammonium compounds on the microbial reductive dechlorination of pentachloroaniline, *Water Res.*, 2013, **47**, 6780–6789.
6 G. A. Kahrilas, J. Blotevogel, P. S. Stewart and T. Borch, Biocides in hydraulic fracturing fluids: a critical review of their usage, mobility, degradation, and toxicity, *Environ. Sci. Technol.*, 2015, **49**, 16–32.
7 X. Li and B. J. Brownawell, Quaternary Ammonium Compounds in Urban Estuarine Sediment Environments – A Class of Contaminants in Need of Increased Attention?, *Environ. Sci. Technol.*, 2010, **44**, 7561–7568.
8 W. T. Stringfellow, J. K. Domen, M. K. Camarillo, W. L. Sandelin and S. Borglin, Physical, chemical, and biological characteristics of compounds used in hydraulic fracturing, *J. Hazard. Mater.*, 2014, **275**, 37–54.
9 A. Butkovskyi, H. Bruning, S. A. E. Kools, H. H. M. Rijnaarts and A. P. Van Wezel, Organic Pollutants in Shale Gas Flowback and Produced Waters: Identification, Potential Ecological Impact, and Implications for Treatment Strategies, *Environ. Sci. Technol.*, 2017, **51**, 4740–4754.
10 M. Elsner and K. Hoelzer, Quantitative Survey and Structural Classification of Hydraulic Fracturing Chemicals Reported in Unconventional Gas Production, *Environ. Sci. Technol.*, 2016, **50**, 3290–3314.
11 J. Yang, U. Tezel, K. Li and S. G. Pavlostathis, Prolonged exposure of mixed aerobic cultures to low temperature and benzalkonium chloride affect the rate and extent of nitrification, *Bioresour. Technol.*, 2015, **179**, 193–201.

12 A. C. Doherty, *The distribution, fate and application as tracers of quaternary ammonium compounds (QACs) in sewage impacted estuaries*, The Graduate School, Stony Brook University, Stony Brook, NY., 2013.
13 T. Ruan, S. Song, T. Wang, R. Liu, Y. Lin and G. Jiang, Identi fi cation and Composition of Emerging Quaternary Ammonium Compounds in Municipal Sewage Sludge in China, *Environ. Sci. Technol.*, 2014, **48**, 4289–4297.
14 E. Martínez-Carballo, C. González-Barreiro, A. Sitka, N. Kreuzinger, S. Scharf and O. Gans, Determination of selected quaternary ammonium compounds by liquid chromatography with mass spectrometry. Part II. Application to sediment and sludge samples in Austria, *Environ. Pollut.*, 2007, **146**, 543–547.
15 A. C. Chiaia-Hernandez, M. Krauss and J. Hollender, Screening of lake sediments for emerging contaminants by liquid chromatography atmospheric pressure photoionization and electrospray ionization coupled to high resolution mass spectrometry, *Environ. Sci. Technol.*, 2013, **47**, 976–986.
16 M. Pateiro-Moure, M. Arias-Estévez and J. Simal-Gándara, Critical Review on the Environmental Fate of Quaternary Ammonium Herbicides in Soils Devoted to Vineyards, *Environ. Sci. Technol.*, 2013, **47**, 4984–4998.
17 X. Li, A. C. Doherty, B. Brownawell and P. A. Lara-Martin, Distribution and diagenetic fate of synthetic surfactants and their metabolites in sewage-impacted estuarine sediments, *Environ. Pollut.*, 2018, **242**, 209–218.
18 P. A. Lara-Martín, X. Li, R. F. Bopp and B. J. Brownawell, Occurrence of alkyltrimethylammonium compounds in urban estuarine sediments: Behentrimonium as a new emerging contaminant, *Environ. Sci. Technol.*, 2010, **44**, 7569–7575.
19 S. G. Pati and W. A. Arnold, Comprehensive screening of quaternary ammonium surfactants and ionic liquids in wastewater effluents and lake sediments, *Environ. Sci.: Processes Impacts*, 2020, **22**, 430–441.
20 X. Li and B. J. Brownawell, Quaternary ammonium compounds in urban estuarine sediment environments – a class of contaminants in need of increased attention?, *Environ. Sci. Technol.*, 2010, **44**, 7561–7568.
21 M. Clara, S. Scharf, C. Scheffknecht and O. Gans, Occurrence of selected surfactants in untreated and treated sewage, *Water Res.*, 2007, **41**, 4339–4348.
22 E. Martínez-Carballo, A. Sitka, C. González-Barreiro, N. Kreuzinger, M. Fürhacker, S. Scharf and O. Gans, Determination of selected quaternary ammonium compounds by liquid chromatography with mass spectrometry. Part I. Application to surface, waste and indirect discharge water samples in Austria, *Environ. Pollut.*, 2007, **145**, 489–496.
23 C. Zhang, U. Tezel, K. Li, D. Liu, R. Ren, J. Du and S. G. Pavlostathis, Evaluation and modeling of benzalkonium chloride inhibition and biodegradation in activated sludge, *Water Res.*, 2011, **45**, 1238–1246.
24 X. Li and B. J. Brownawell, Analysis of quaternary ammonium compounds in estuarine sediments by LC-ToF-MS: Very high positive mass defects of alkylamine ions as powerful diagnostic tools for identification and structural elucidation, *Anal. Chem.*, 2009, **81**, 7926–7935.
25 I. Ferrer and E. M. Thurman, Analysis of hydraulic fracturing additives by LC/Q-TOF-MS, *Anal. Bioanal. Chem.*, 2015, **407**, 6417–6428.
26 I. Ferrer and E. T. Furlong, Identification of alkyl dimethylbenzylammonium surfactants in water samples by solid-phase extraction followed by ion trap LC/MS and LC/MS/MS, *Environ. Sci. Technol.*, 2001, **35**, 2583–2588.
27 *Antimicrobial Resistance in the Environment*, ed. P. L. Keen and M. H. M. M. Montforts, John Wiley & Sons, Inc., Hoboken, NJ, USA, 2011.
28 M. Kim, M. R. Weigand, S. Oh, J. K. Hatt, R. Krishnan, U. Tezel, S. G. Pavlostathis and K. T. Konstantinidis, Widely used benzalkonium chloride disinfectants can promote antibiotic resistance, *Appl. Environ. Microbiol.*, 2018, **84**, e01201–18.
29 M. C. Jennings, K. P. C. Minbiole and W. M. Wuest, Quaternary Ammonium Compounds: An Antimicrobial Mainstay and Platform for Innovation to Address Bacterial Resistance, *ACS Infect. Dis.*, 2015, **1**, 288–303.
30 H. Sütterlin, R. Alexy, A. Coker and K. Kümmerer, Mixtures of quaternary ammonium compounds and anionic organic compounds in the aquatic environment: Elimination and biodegradability in the closed bottle test monitored by LC-MS/MS, *Chemosphere*, 2008, **72**, 479–484.
31 M. T. García, E. Campos, J. Sánchez-Leal and I. Ribosa, Anaerobic degradation and toxicity of commercial cationic surfactants in anaerobic screening tests, *Chemosphere*, 2000, **41**, 705–710.
32 M. T. García, I. Ribosa, T. Guindulain, J. Sánchez-Leal and J. Vives-Rego, Fate and effect of monoalkyl quaternary ammonium surfactants in the aquatic environment, *Environ. Pollut.*, 2001, **111**, 169–175.
33 U. Tezel, M. Tandukar, R. J. Martinez, P. A. Sobecky and S. G. Pavlostathis, Aerobic Biotransformation of *n*-Tetradecylbenzyldimethylammonium Chloride by an Enriched Pseudomonas spp. Community, *Environ. Sci. Technol.*, 2012, **46**, 8714–8722.
34 E. Ertekin, K. T. Konstantinidis and U. Tezel, A Rieske-Type Oxygenase of *Pseudomonas* sp. BIOMIG1 Converts Benzalkonium Chlorides to Benzyldimethyl Amine, *Environ. Sci. Technol.*, 2017, **51**, 175–181.
35 E. Ertekin, J. K. Hatt, K. T. Konstantinidis and U. Tezel, Similar Microbial Consortia and Genes Are Involved in the Biodegradation of Benzalkonium Chlorides in Different Environments, *Environ. Sci. Technol.*, 2016, **50**, 4304–4313.
36 Y. J. S. Lai, A. Ontiveros-Valencia, Z. E. Ilhan, Y. Zhou, E. Miranda, J. Maldonado, R. Krajmalnik-Brown and B. E. Rittmann, Enhancing biodegradation of C16-alkyl quaternary ammonium compounds using an oxygen-based membrane biofilm reactor, *Water Res.*, 2017, **123**, 825–833.
37 S. T. J. Droge and K. U. Goss, Ion-exchange affinity of organic cations to natural organic matter: influence of amine type and nonionic interactions at two different pHs, *Environ. Sci. Technol.*, 2013, **47**, 798–806.

38 B. J. Brownawell, H. Chen, J. M. Collier and J. C. Westall, Adsorption of organic cations to natural materials, *Environ. Sci. Technol.*, 1990, **24**, 1234–1241.
39 N. Kreuzinger, M. Fuerhacker, S. Scharf, M. Uhl, O. Gans and B. Grillitsch, Methodological approach towards the environmental significance of uncharacterized substances – quaternary ammonium compounds as an example, *Desalination*, 2007, **215**, 209–222.
40 K. Jardak, P. Drogui and R. Daghrir, Surfactants in aquatic and terrestrial environment: occurrence, behavior, and treatment processes, *Environ. Sci. Pollut. Res.*, 2016, **23**, 3195–3216.
41 W. H. Gaze, N. Abdouslam, P. M. Hawkey and E. M. H. Wellington, Incidence of Class 1 Integrons in a Quaternary Ammonium Compound-Polluted Environment, *Antimicrob. Agents Chemother.*, 2005, **49**, 1802–1807.
42 M. R. Gillings, Integrons: past, present, and future, *Microbiol. Mol. Biol. Rev.*, 2014, **78**, 257–277.
43 M. R. Gillings, M. P. Holley and H. W. Stokes, Evidence for dynamic exchange of qac gene cassettes between class 1 integrons and other integrons in freshwater biofilms, *FEMS Microbiol. Lett.*, 2009, **296**, 282–288.
44 M. R. Gillings, D. Xuejun, S. A. Hardwick, M. P. Holley and H. W. Stokes, Gene cassettes encoding resistance to quaternary ammonium compounds: a role in the origin of clinical class 1 integrons?, *ISME J.*, 2009, **3**, 209–215.
45 I. Mulder, J. Siemens, V. Sentek, W. Amelung, K. Smalla and S. Jechalke, Quaternary ammonium compounds in soil: implications for antibiotic resistance development, *Rev. Environ. Sci. Bio/Technol.*, 2018, **17**, 159–185.
46 United States Environmental Protection Agency Office of Prevention, Pesticides and Toxic Substances, *Reregistration Eligibility Decision for Alkyl Dimethyl Benzyl Ammonium Chloride (ADBAC)*, Washington, DC, 2006.
47 M. E. Karpuzcu, A. J. McCabe and W. A. Arnold, Phototransformation of pesticides in prairie potholes: effect of dissolved organic matter in triplet-induced oxidation, *Environ. Sci.: Processes Impacts*, 2016, **18**, 237–245.
48 T. Zeng and W. A. Arnold, Pesticide Photolysis in Prairie Potholes: Probing Photosensitized Processes, *Environ. Sci. Technol.*, 2013, **47**, 6735–6745.
49 A. J. McCabe and W. A. Arnold, Reactivity of Triplet Excited States of Dissolved Natural Organic Matter in Stormflow from Mixed-Use Watersheds, *Environ. Sci. Technol.*, 2017, **51**, 9718–9728.
50 S. E. Page, W. A. Arnold and K. McNeill, Assessing the Contribution of Free Hydroxyl Radical in Organic Matter-Sensitized Photohydroxylation Reactions, *Environ. Sci. Technol.*, 2011, **45**, 2818–2825.
51 M. Grandbois, D. E. Latch and K. McNeill, Microheterogeneous Concentrations of Singlet Oxygen in Natural Organic Matter Isolate Solutions, *Environ. Sci. Technol.*, 2008, **42**, 9184–9190.
52 A. Leifer, *The Kinetics of Environmental Aquatic Photochemistry: Theory and Practice*, American Chemical Society, Washington, DC, 1988.
53 D. Dulin and T. Mill, Development and evaluation of sunlight actinometers, *Environ. Sci. Technol.*, 1982, **16**, 815–820.
54 K. McNeill and S. Canonica, Triplet state dissolved organic matter in aquatic photochemistry: reaction mechanisms, substrate scope, and photophysical properties, *Environ. Sci.: Processes Impacts*, 2016, **18**, 1381–1399.
55 J. E. Grebel, J. J. Pignatello and W. A. Mitch, Effect of halide ions and carbonates on organic contaminant degradation by hydroxyl radical-based advanced oxidation processes in saline waters, *Environ. Sci. Technol.*, 2010, **44**, 6822–6828.
56 J. E. Grebel, J. J. Pignatello and W. A. Mitch, Sorbic acid as a quantitative probe for the formation, scavenging and steady-state concentrations of the triplet-excited state of organic compounds, *Water Res.*, 2011, **45**, 6535–6544.
57 G. V. Buxton, C. L. Greenstock, W. P. Helman and A. B. Ross, Critical Review of rate constants for reactions of hydrated electrons, hydrogen atoms and hydroxyl radicals ($^{\bullet}OH/^{\bullet}O^-$ in Aqueous Solution, *J. Phys. Chem. Ref. Data*, 1988, **17**, 513–886.
58 E. Appiani, R. Ossola, D. E. Latch, P. R. Erickson and K. McNeill, Aqueous singlet oxygen reaction kinetics of furfuryl alcohol: effect of temperature, pH, and salt content, *Environ. Sci.: Processes Impacts*, 2017, **19**, 507–516.
59 NREL, *SMARTS: Simple Model of the Atmospheric Radiative Transfer of Sunshine*, https://www.nrel.gov/grid/solar-resource/smarts.html, accessed 6 September 2019.
60 C. A. Gueymard, Parameterized transmittance model for direct beam and circumsolar spectral irradiance, *Sol. Energy*, 2001, **71**, 325–346.
61 C. Gueymard, *SMARTS2, A Simple Model of the Atmospheric Radiative Transfer of Sunshine: Algorithms and Performance Assessment*, Florida Solar Energy Center, 1995.
62 J. R. Laszakovits, S. M. Berg, B. G. Anderson, J. E. O'Brien, K. H. Wammer and C. M. Sharpless, p-Nitroanisole/Pyridine and p-Nitroacetophenone/Pyridine Actinometers Revisited: Quantum Yield in Comparison to Ferrioxalate, *Environ. Sci. Technol. Lett.*, 2017, **4**, 11–14.
63 S. G. Pati and W. A. Arnold, Photochemical Transformation of Four Ionic Liquid Cation Structures in Aqueous Solution, *Environ. Sci. Technol.*, 2017, **51**, 11780–11787.
64 R. P. Schwarzenbach, P. M. Gschwend and D. M. Imboden, *Environmental Organic Chemistry*, John Wiley & Sons, Inc., Hoboken, NJ, USA, 2002.
65 D. E. Latch, in *Surface Water Photochemistry*, The Royal Society of Chemistry, 2015, pp. 139–165.
66 W. A. Arnold and K. McNeill, Transformation of pharmaceuticals in the environment: Photolysis and other abiotic processes, in *Comprehensive Analytical Chemistry*, Elsevier, 2007, vol. 50, pp. 361–385.
67 F. L. Rosario-Ortiz and S. Canonica, Probe Compounds to Assess the Photochemical Activity of Dissolved Organic Matter, *Environ. Sci. Technol.*, 2016, **50**, 12532–12547.
68 M. Minella, L. Rapa, L. Carena, M. Pazzi, V. Maurino, C. Minero, M. Brigante and D. Vione, An experimental methodology to measure the reaction rate constants of processes sensitised by the triplet state of 4-

carboxybenzophenone as a proxy of the triplet states of chromophoric dissolved organic matter, under steady-state irradiation conditions, *Environ. Sci.: Processes Impacts*, 2018, **20**, 1007–1019.

69 F. al Housari, D. Vione, S. Chiron and S. Barbati, Reactive photoinduced species in estuarine waters. Characterization of hydroxyl radical, singlet oxygen and dissolved organic matter triplet state in natural oxidation processes, *Photochem. Photobiol. Sci.*, 2010, **9**, 78–86.

70 S. G. Pavlostathis, T. Konstantinidis, S. Oh, Z. Kurt, D. Tsementzi, M. R. Weigand, M. Kim, J. K. Hatt, M. Tandukar, S. G. Pavlostathis, J. C. Spain and K. T. Konstantinidis, Microbial Community Degradation of Widely Used Quaternary Ammonium Disinfectants, *Appl. Environ. Microbiol.*, 2014, **80**, 5892–5900.

71 J. Wenk, U. von Gunten and S. Canonica, Effect of Dissolved Organic Matter on the Transformation of Contaminants Induced by Excited Triplet States and the Hydroxyl Radical, *Environ. Sci. Technol.*, 2011, **45**, 1334–1340.

72 M. W. Lam and S. A. Mabury, Photodegradation of the pharmaceuticals atorvastatin, carbamazepine, levofloxacin, and sulfamethoxazole in natural waters, *Aquat. Sci.*, 2005, **67**, 177–188.

73 P. L. Brezonik and J. Fulkerson-Brekken, Nitrate-Induced Photolysis in Natural Waters: Controls on Concentrations of Hydroxyl Radical Photo-Intermediates by Natural Scavenging Agents, *Environ. Sci. Technol.*, 1998, **32**, 3004–3010.

74 R. G. Zepp, J. Hoigne and H. Bader, Nitrate-induced photooxidation of trace organic chemicals in water, *Environ. Sci. Technol.*, 1987, **21**, 443–450.